Comparison of PI and ADRC Current Controllers for IFOC-Driven Synchronous Reluctance Motors

Kevin Ramos-Bravo * **Aron Belizario** * **Danny G. Lopez** *
José L. Azcue *

* *Graduate Program in Electrical Engineering,*
Federal University of ABC (UFABC).
e-mail: {k.bravo,aron.belizario,danny.lopez,jose.azcue}@ufabc.edu.br

Abstract: Currently, electric motors are used in various industrial applications and electric vehicles, leading to increased research and development in efficient propulsion systems and cost-effective design. Reluctance synchronous motors (SynRM) are among alternating current electric machines, owing to their simple and robust design. The objective of the article is to design a high-performance control system. Initially, the indirect field-oriented control using PI controllers will be implemented for driving the SynRM. Subsequently, these controllers will be replaced by controllers with active disturbance rejection (ADRC). Simulation for this control system is conducted using Matlab/Simulink software. Finally, the results show better performance from the ADRC current controller than the PI controllers. The ADRC provides faster response times, better tracking capabilities, real-time disturbance rejection, and reduced ripples.

Keywords: Reluctance synchronous motor, IFOC, PI control, ADRC control, high performance, stability.

1. INTRODUCTION

In recent years, SynRM has proven to be competitive in drive systems alongside other types of electric machines, such as synchronous and asynchronous alternating current motors. It has garnered attention in industries for its high efficiency, low costs, simple structure, and robustness (Bao et al., 2021) - (Farhan et al., 2013).

The rotor of SynRM, due to its simple structure, is not constituted by a squirrel cage like induction motors, nor a field or permanent magnet excitation winding (Imen et al., 2016), but generally exists in three types: segmental, flux-bar, and axially laminated (Farhan et al., 2013), while the stator structure is similar to that of an induction machine with a cylindrical inner surface and windings. Additionally, SynRM presents advantages in its high operational efficiency, easy maintenance, low rotor losses due to the absence of windings, and simple control schemes (Dursun et al., 2022), making it suitable for various applications in the industrial and automotive sectors (Farhan et al., 2013).

In the design of the motor behind its simultaneous advancement of the geometric rotor and the drive systems in the power electronics, high-performance SynRM studies were developed, using systems of "maximum torque control, response control fast pair control, maximum efficiency control, maximum power factor control, constant current control of the axis d and field weakening control", as well as using different methods (Dursun et al., 2022). Field oriented control (FOC) is one of them in Imen et al. (2016), which uses traditional PI controllers in the SynRM drive system.

The PI parameters depend on the inductance in the motor axes (Ld, Lq) and the stator resistance Rs. When the SynRM comes into operation, it increases the temperature, and the magnetic circuit saturation tends to change the Ld, Lq, and Rs, obtaining poor and unstable operation. An alternative to traditional PI controllers is Active Disturbance Rejection Control (ADRC) (Han, 2009), which has shown promising results in motor drive systems. In Accetta et al. (2020), ADRC was successfully used to control the flux linkage and speed of a SynRM, demonstrating good performance. ADRC also proved effective in controlling a PMSM servo system in Guo et al. (2017), by rejecting internal and external disturbances. This is because the controller does not rely on the mathematical model of the plant (Li et al., 2021).

This article presents the current control method of the SynRM using ADRC controllers instead of the traditional PI controllers. Compared to PI controllers, the SynRM drive system performance with ADRC is superior, demonstrating good tracking capabilities and mitigating system disturbances.

This article describes in Section II the SynRM and the mathematical model through the equations. Section III describes the control strategy and controller design of the SynRM. Section IV shows the simulation results to validate the proposed strategy. Finally, in section V, the conclusions of the article are presented.

2. SYNCHRONOUS RELUTANCE MOTOR

In Di Nardo et al. (2017) the SynRM, compared topologically with other high-speed machines in AC, these being the IM, PMSM and SRM, has the following advantages:

- Not requiring retention systems or complex constructions on the rotor. Which would cause losses in efficiency in the operation and economic costs.
- High efficiency and torque density, unlike PMSMs that require rare earth Permanent Magnets.

The operation of SynRM occurs in relation to reluctance variation, where magnetic resistance changes based on the rotor's position relative to the stator. When the stator is energized, the generated magnetic flux flows through the rotor section with the lowest magnetic resistance, causing the rotor to align itself with this position of least reluctance (Kumar et al., 2023).

2.1 Mathematical Modeling of Synchronous Reluctance Motor

The mathematical equations (1) and (2) of the SynRM are analyzed and obtained using the equivalent model of the electrical circuit on the rotational reference axes in the steady state of two phases $d-q$, and are shown in Fig. 1.

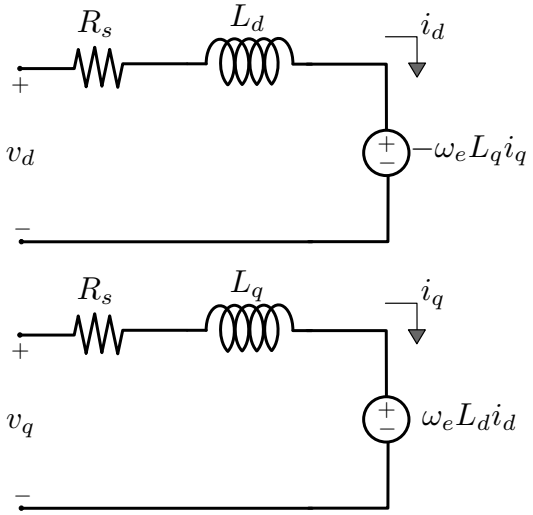

Figure 1. SynRM equivalent circuit in the d-q frame.

$$v_d = R_s i_d + L_d \frac{di_d}{dt} - \omega_e L_q i_q \tag{1}$$

$$v_q = R_s i_q + L_q \frac{di_q}{dt} + \omega_e L_d i_d \tag{2}$$

Where v_d and v_q are stator voltages on the d and q axis, i_d and i_q are the stator currents on the d and q axis, L_d and L_q are the stator inductances on the d and q axis, R_s is the stator resistance and ω_e is the electrical angular speed of the rotor.

The dynamic equations (3) and (4) of the electromagnetic torque are given in the following equations:

$$T_e = \frac{3}{2} p (L_d - L_q) I_d I_q \tag{3}$$

$$T_e - T_L = J_m \frac{d\omega_r}{dt} + B_m \omega_r \tag{4}$$

Where T_e is electromagnetic torque, T_L is the load torque, p is the number of pole pairs, ω_r is the mechanical angular speed of the rotor, J_m is the moment of inertia of the rotor, B_m is the viscosity coefficient.

Fig. 2. shows the block diagram representing the dynamic model of the SynRM. Considering the $d-q$ reference framework it was obtained the following equations (5), (6), (7) and (8):

$$\frac{d}{dt} i_d = \frac{1}{L_d} (v_d - R_s i_d + \omega_e L_q i_q) \tag{5}$$

$$\frac{d}{dt} i_q = \frac{1}{L_q} (v_q - R_s i_q - \omega_e L_d i_d) \tag{6}$$

$$\frac{d}{dt} \omega_r = \frac{1}{J_m} (T_e - T_L - B_m \omega_r) \tag{7}$$

$$\frac{d\theta_e}{dt} = \omega_e = p \omega_r \tag{8}$$

Where θ_e is the electrical angle of the rotor.

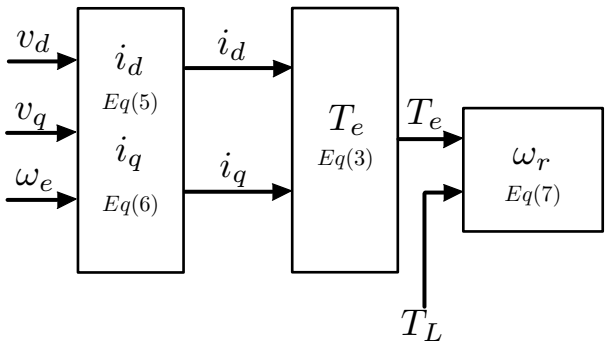

Figure 2. SynRM block diagram.

3. DESIGN OF THE CONTROL STRATEGY FOR SYNRM

The control strategy for SynRMs, due to its various advantages such as minimal torque ripple and simplicity of operation adaptation, is the Field Oriented Control (FOC) strategy, but it suffers from internal and external disturbances, also with the dynamic response which is slow (Kumar et al., 2023). In Fig. 3, the IFOC control scheme is shown.

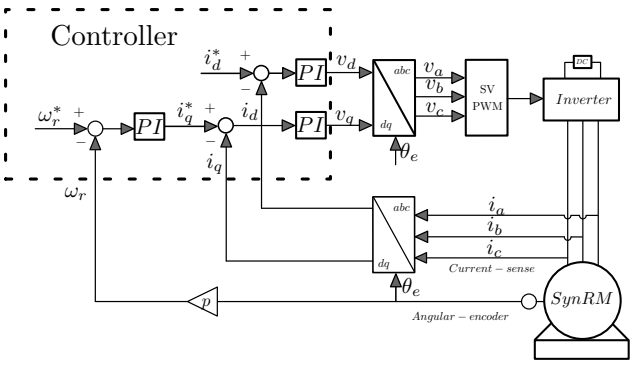

Figure 3. Block diagram of IFOC control for SynRM

3.1 PI controller for current and speed loop

In Scalcon et al. (2019), calculations are performed by determining the transfer functions for the current and speed controller gains.

PI current controller

The transfer function (9) of the PI controller and the transfer function (10) of the electrical model of the SynRM are defined by the following equations in the $d-q$ reference frame.

$$G_{C_{d,q}}(s) = k_{p_{d,q}} + \frac{k_{i_{d,q}}}{s} \tag{9}$$

$$G_{d,q}(s) = \frac{\frac{1}{L_{d,q}}}{s + \frac{R_s}{L_{d,q}}} \tag{10}$$

Where $k_{p_{d,q}}$ and $k_{i_{d,q}}$ are the proportional and integral gains, $L_{d,q}$ are the inductances in the $d-q$ reference frames.

Transfer functions (11), (12) and (13) of the I_d and I_q currents in a closed loop are defined by.

$$G_{mf_{d,q}} = \frac{G_{C_{d,q}}(s)G_{d,q}(s)}{1 + G_{C_{d,q}}(s)G_{d,q}(s)} \tag{11}$$

$$G_{mf_{d,q}} = \frac{\frac{k_{p_{d,q}}}{L_{d,q}} + \frac{k_{i_{d,q}}}{L_{d,q}}}{s^2 + \frac{R_s + k_{p_{d,q}}}{L_{d,q}}s + \frac{k_{i_{d,q}}}{L_{d,q}}} \tag{12}$$

$$G_{mf_{d,q}} = \frac{2\xi_{1,2}\omega_{C_{d,q}}s + \omega_{C_{d,q}}^2}{s^2 + 2\xi_{C_{d,q}}\omega_{C_{d,q}}s + \omega_{C_{d,q}}^2} \tag{13}$$

Where $\xi_{C_{d,q}}$ are the desired damping coefficients for the system, $\xi_{1,2}$ are the damping coefficients obtained from the equality of the denominator, and $\omega_{C_{d,q}}$ are the undamped natural frequencies, in the $d-q$ reference frame.

The adjustment parameters $k_{p_{d,q}}$ and $k_{i_{d,q}}$ of the PI current controllers are determined by (14) and (15).

$$k_{p_{d,q}} = 2\xi_{1,2}\omega_{C_{d,q}}L_{d,q} - R_s \tag{14}$$

$$k_{i_{d,q}} = \omega_{C_{d,q}}^2 L_{d,q} \tag{15}$$

PI speed controller

The transfer function (16) of the PI controller and the transfer function (17) of the mechanical model of the SynRM are defined by.

$$G_{C_{\omega_r}}(s) = k_{p_{\omega_r}} + \frac{k_{i_{\omega_r}}}{s} \tag{16}$$

$$G_{\omega_r}(s) = \frac{\frac{1}{J_m}}{s + \frac{B_m}{J_m}} \tag{17}$$

Where $k_{p_{\omega_r}}$ and $k_{i_{\omega_r}}$ are the proportional and integral gains, $L_{d,q}$ are the inductances in the $d-q$ reference frames.

The transfer functions $G_{mf_{d,q}}(s)$ of the speed ω_r in a closed loop, is carried out analogously to that of the current loop.

The adjustment parameters $k_{p_{\omega_r}}$ and $k_{i_{\omega_r}}$ of the PI speed controllers are determined by the equations (18) and (19),

$$k_{p_{\omega_r}} = 2\xi_3\omega_{C_{\omega_r}}J_m - B_m \tag{18}$$

$$k_{i_{\omega_r}} = \omega_{C_{\omega_r}}^2 J_m \tag{19}$$

Where ξ_3 are the damping coefficients obtained from the equality of the denominator, and $\omega_{C_{\omega_r}}$ are the undamped natural frequencies, in the $d-q$ reference frame.

3.2 ADRC-Based Control Strategy

For the ADRC design, only the plant order and estimation of the input gain b_0 are required. Also, for it to perform well in terms of disturbance rejection compared to PI controllers, an accurate estimate of disturbances is attributed through the Extended State Observer (ESO) (Han, 2009) and (Abdellah Oukassi, 2024).

A Single Input - Single Output (SISO) system is considered for ESO's design (Han, 2009) and (Zhou and Gao, 2007) described (20):

$$\dot{x} = f(x,t) + \omega(t) + b_0u_0 \tag{20}$$

Where x is the state variable, $f(x,t)$ is the internal dynamics of the system, $\omega(t)$ is the unknown disturbance, b_0 is the parameter of the system and u_0 is the input of the system.

If $d(t) = f(x,t) + \omega(t)$ is the grouped perturbation, by extending it as a new state, the following system (21) is obtained:

$$\begin{cases} \dot{x_1} = x_2 + b_0u_0 \\ \dot{x_2} = \dot{d(t)} \end{cases} \tag{21}$$

where $x_1 = x$ and $x_2 = d(t)$. Therefore, the ESO (22) is written as follows:

$$\begin{cases} \varepsilon = z_1 - x_1 \\ \dot{z_1} = z_2 - \beta_1\varepsilon + f + b_0u \\ \dot{z_2} = -\beta_2\varepsilon \end{cases} \tag{22}$$

where ε is the estimated error, x_1 is the actual state variable, z_1 is the estimated state variable, z_2 is the estimated unknown perturbation, f is the known perturbation, β_1 and β_2 are the gains of the ESO.

The dynamics of the ESO error (23) are written according to the equations (21) and (22).

$$\ddot{\varepsilon_1} = \ddot{z_1} - \ddot{x_1} = -\beta_1\dot{\varepsilon_1} - \beta_2\varepsilon_1 - \dot{d(t)} \tag{23}$$

where $\ddot{\varepsilon_1}$ is the second-order derivative and $\dot{\varepsilon_1}$ is the first-order derivative of ε_1. Then the concentrated disturbances are written in the frequency domain (24) as follows:

$$\frac{z_2(s)}{x_2(s)} = \frac{\beta_2}{s^2 + \beta_1 s + \beta_2} \tag{24}$$

According to the equation (24), it conclude that the transfer function x_2 on z_2 does not depend on the dynamic model and system parameters. The gain of the ESO, that is, β_1 and β_2, are independent of the system.

Current ADRC-based controller

Two current ADRC-based controllers were utilized to regulate the I_d and I_q currents. For the design of the ESO, from the equations (1) and (2), the disturbances of the current in the d axis are known, where $f_d = -R_s i_d/L_d + L_q \omega_e i_q/L_d$ and on the q axis $f_q = -R_s i_q/L_q - L_d \omega_e i_d/L_q$. Then the design of the ESO is known according to the equations (25) and (26).

$$\begin{cases} \varepsilon_d = \hat{i}_d - i_d \\ \dot{\hat{i}}_d = z_d + f_d + \dfrac{v_d}{L_d} - \beta_{d1}\varepsilon_d \\ f_d = -\dfrac{R_s}{L_d} i_d + \dfrac{L_q}{L_d}\omega_e i_q \\ \dot{z}_d = -\beta_{d2}\varepsilon_d \end{cases} \tag{25}$$

$$\begin{cases} \varepsilon_q = \hat{i}_q - i_q \\ \dot{\hat{i}}_q = z_q + f_q + \dfrac{v_q}{L_q} - \beta_{q1}\varepsilon_q \\ f_q = -\dfrac{R_s}{L_q} i_q - \dfrac{L_d}{L_q}\omega_e i_d \\ \dot{z}_q = -\beta_{q2}\varepsilon_q \end{cases} \tag{26}$$

Where ε_d and ε_q are the error estimates, $\hat{i}_d$ and $\hat{i}_q$ are the current estimates, f_d and f_q are the known disturbances, z_d and z_q are the unknown perturbations and β_{d1}, β_{d2}, β_{q1} and β_{q2} are the ESO gains.

To adjust the parameters of the ESO gains in Zhou and Gao (2007), they are adjusted according to the transfer function, where $\beta_{d1} = \beta_{q1} = 2\omega_o$ and $\beta_{d2} = \beta_{q2} = \omega_o^2$.

The ω_o is the observability bandwidth, it can be calculated based on the ω_c which is the control bandwidth, as $\omega_o = (3 \sim 5)\omega_c$. When ω_o is a maximum value, it tends to generate too much noise, but when it is a minimum value, it tends to converge slowly.

Implementation of the ADRC for the IFOC control system

The block diagram of the ADRC-based IFOC control method is shown in Figure 4. ADRC compensates for disturbances accumulated in the system, so to achieve the desired control, a simple proportional controller is applied according to equations (27) and (28).

$$v_{d0} = k_d(i_d - \hat{i}_d) \tag{27}$$

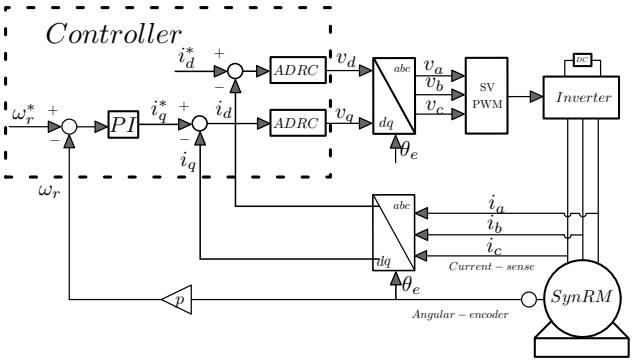

Figure 4. Block diagram of IFOC strategy based on ADRC controllers

$$v_{q0} = k_q(i_q - \hat{i}_q) \tag{28}$$

Where $k_d = k_q = \omega_c$, are the controller gains of the currents i_d and i_q. The Fig. 5 shows the design of the ADRC.

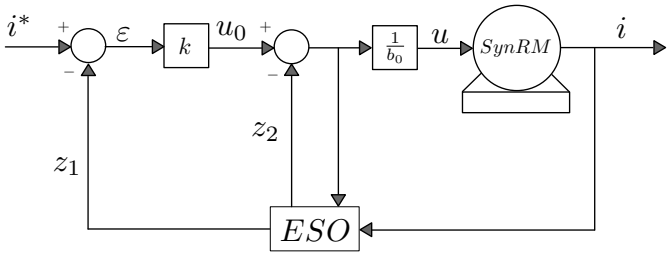

Figure 5. ADRC block diagram.

According to ADRC, a law of control is then determined by the equations (29) and (30) which show the voltage outputs on the $d-q$ axis.

$$v_d = \frac{v_{d0} - (z_d + f_d)}{L_d} \tag{29}$$

$$v_q = \frac{v_{q0} - (z_q + f_q)}{L_q} \tag{30}$$

4. SIMULATION AND RESULTS

The SynRM parameters are shown in Table 1. This section shows the results obtained from the simulation with Matlab/Simulink software, and the performance of the IFOC method was analyzed using the PI and the ADRC controllers. The numerical simulation is carried out in discrete time, considering a sampling period $T_s = 5\mu s$ and a switching frequency of $f_s = 8kHz$.

4.1 Simulation results with speed reference variation with no-load

In Figures 6, 7, and 8, the performance of the PI and ADRC controllers is shown in relation to the currents, I_d and I_q, in the $d-q$ axes and the rotor speed ω_r. A current $i_d^* = 3A$ is considered. Also, for the simulation, the reference speeds of $20rad/s$, $50rad/s$, and $30rad/s$ are considered at times $1s$, $3s$, and $5s$, respectively.

Table 1. SynRM parameters and rated values

Parameters	*Symbol*	*Value*	*Unit*
Stator resistance	R_s	2.4077	Ω
Inductance of axis d	L_d	0.32689	H
Inductance of axis q	L_q	0.09436	H
Rotor moment of inertia	J_m	0.004	$kg.m^2$
Viscous Coefficient	B_m	0.006	Nms/rad
Number of pole pairs	p	2	
Rated Voltage	V_{cc}	400	V
Rated Current	I_n	5	A
Rated Power	P	2.2	kW
Rated Speed	ω_n	1500	RPM

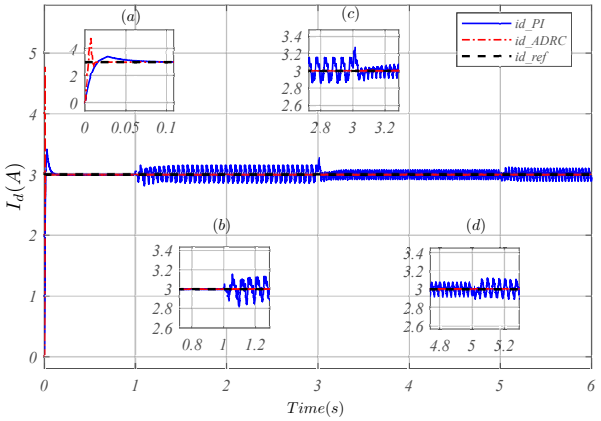

Figure 6. The control of the I_d-axis current with a constant reference.

In Figure 6, it is observed that the response time of the ADRC controller is faster than that of the PI controller, stabilizing in a time of $0.01s$, while the PI controller stabilizes in a time of $0.1s$. In Figures 6 (b), (c) e (d), 7 (a), (b) e (c), and 8 (a), (b) e (c) prolonged oscillations of the PI controller are observed, which are greater than those of the ADRC controller, which remains constant.

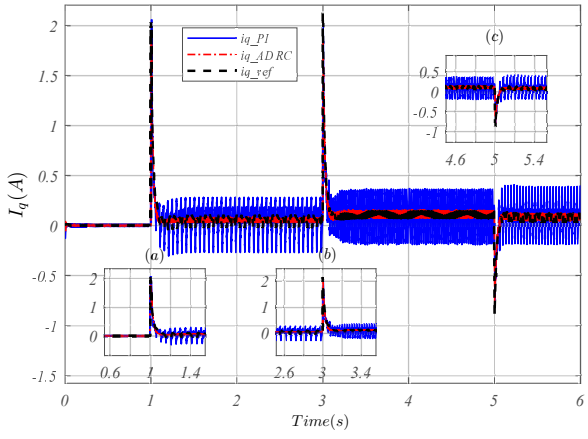

Figure 7. The control of the I_q-axis current with a variable reference.

Table 2 shows the comparison of the current ripple values, which is calculated as the difference between the maximum and minimum value in a given interval ($\Delta I_{d,q} = I_{d,q}max - I_{d,q}min$). So, the ADRC controller shows better performance.

Table 2. Comparison of the current ripple

Speed	Ripples Δ I_d (A)		Ripples Δ I_q (A)	
(rad/s)	***PI***	***ADRC***	***PI***	***ADRC***
20	0.285	0.017	0.517	0.073
50	0.116	0.017	0.479	0.073
30	0.209	0.017	0.545	0.073

In Figure 8, shows the IFOC method with the current PI controller tracking the speed reference. At $1s$, there is an overshoot when the speed is $20rad/s$. The overshoot continues until $1.4s$, and then the system stabilizes with ripples until $3s$. Similar behavior is observed at both $3s$ and $5s$ in terms of overshoot and ripples.

On the other hand, the IFOC method with the current ADRC controller reacts similarly to the PI controllers but eliminates ripples and maintains stable control.

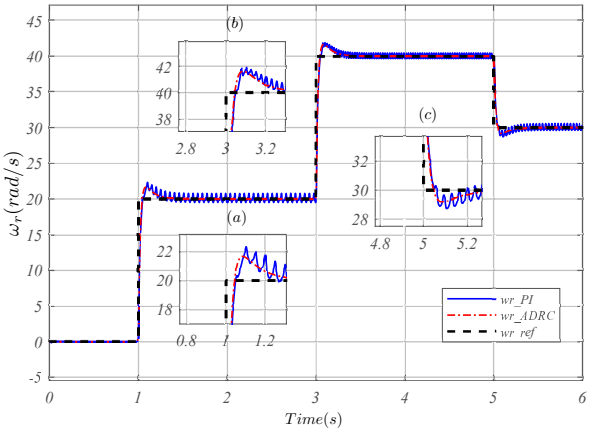

Figure 8. Speed control ω_r, with reference variation.

4.2 Simulation results with speed reference constant and with load

In Figures 9, 10, and 11, show the behavior of the currents I_q and I_d, and the rotor speed ω_r when the PI and ADRC controllers are used. A $2Nm$ load is applied from $2s$ to $4s$ with a reference speed of $\omega_r = 100rad/s$.

In Figure 9 (a), it can be observed that the response time of the I_q current is faster when the ADRC controller is used, in this case the current stabilizes at $0.018s$, while it stabilizes at $0.17s$ when the PI controller is used.

In Figures 9 (b) e 9 (c) it's also noticeable that during the load period from $2s$ to $4s$, the ADRC controller can maintain the I_q current constant without any disturbance, while the PI controller cannot reject the disturbances appropriately.

In Figure 10 it is observed that the current I_q follows the references precisely.

In Figure 11 (a) shows the behavior of the PI controller tracking the speed reference. Note that the same PI speed controller was used for both cases, IFOC with PI and with ADRC controllers. For this reason, the speed responses are similar.

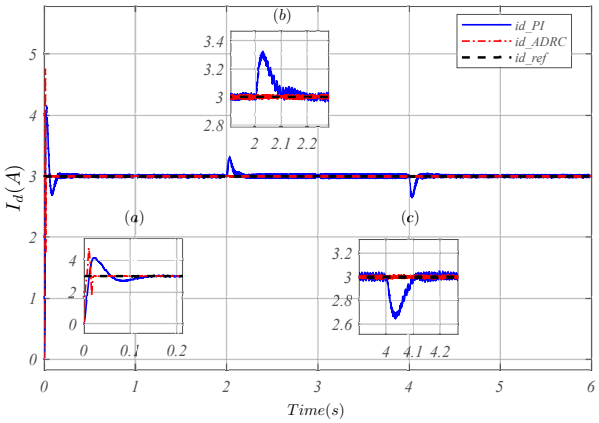

Figure 9. Current control I_d on axis d, with load.

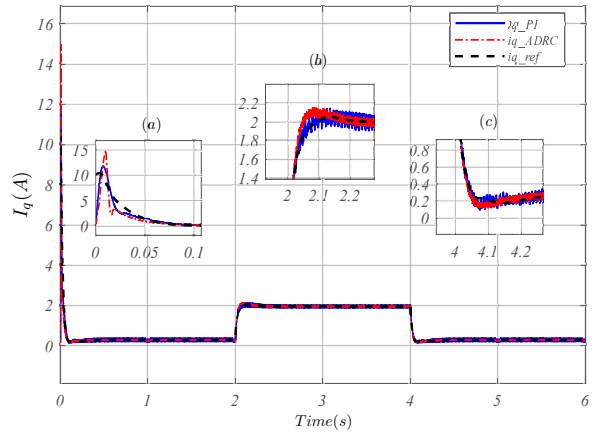

Figure 10. Current control I_q on axis q, with load.

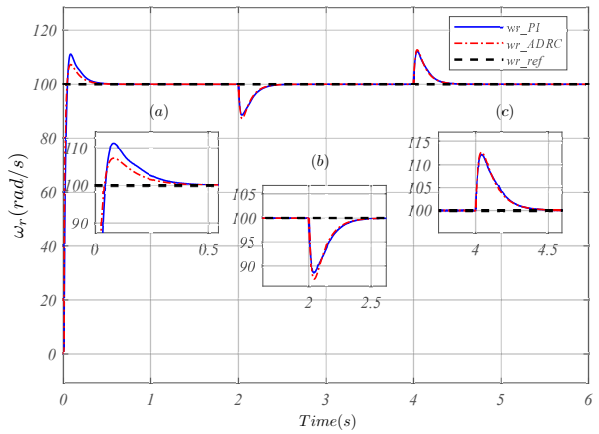

Figure 11. Speed control ω_r, with load.

5. CONCLUSION

In this article, two ADRC current controllers were designed, to replace the PI controllers present in the IFOC vector control used to drive the SynRM. It was verified through simulations in Matlab/Simulink that the ADRC controller was able to control the currents Id and Iq with a smaller ripple when compared to the PI controller when a constant speed was considered. Furthermore, with the ADRC controller, the Id, and Iq currents followed the references precisely and effectively rejected disturbances when the 2Nm load was applied.

ACKNOWLEDGMENT

This study was financed in part by the Coordenação de Aperfeiçoamento de Pessoal de Nível Superior – Brasil (CAPES) – Finance Code 001.

REFERENCES

Abdellah Oukassi, Oumaymah Elamri, Z.B. (2024). Adrc and ifoc control of a sensorless induction motor driven by a multilevel converter using svm approach and pv generators. *Mathematical Problems in Engineering*, 2024, 15.

Accetta, A., Cirrincione, M., D'Ippolito, F., Pucci, M., and Sferlazza, A. (2020). Active disturbance rejection control of synchronous reluctance motors. In *2020 IEEE Energy Conversion Congress and Exposition (ECCE)*.

Bao, Z., Wei, S., and Dong, J. (2021). Speed sensorless control of synchronous reluctance motor at full speed range. In *2021 IEEE 4th International Electrical and Energy Conference (CIEEC). IEEE.*

Di Nardo, M., Calzo, G.L., Galea, M., and Gerada, C. (2017). Design optimization of a high-speed synchronous reluctance machine. *IEEE Transactions on Industry Applications*, 54(1), 233–243.

Dursun, D.C., Yildiz, A., and Polat, M. (2022). Modeling of synchronous reluctance motor and open and closed loop speed control. In *2022 21st International Symposium INFOTEH-JAHORINA (INFOTEH)*, 1–6. IEEE.

Farhan, A., Saleh, A., and Shaltout, A. (2013). High performance reluctance synchronous motor drive using field oriented control. In *2013 5th International Conference on Modelling, Identification and Control (ICMIC)*, 181–186. IEEE.

Guo, B., Bacha, S., and Alamir, M. (2017). A review on adrc based pmsm control designs. In *IECON 2017-43rd annual conference of the IEEE industrial electronics society*, 1747–1753. IEEE.

Han, J. (2009). From pid to active disturbance rejection control. *IEEE transactions on Industrial Electronics*, 56(3), 900–906.

Imen, T., Amor, K., Oussamal, S., Abdelkader, C., and Mohamed, B. (2016). Performance analysis of foc and dtc for synchronous reluctance motor. In *2016 17th International Conference on Sciences and Techniques of Automatic Control and Computer Engineering (STA)*, 260–264. IEEE.

Kumar, H., Kumar, A., et al. (2023). Foc based control of a synrm for space application. In *2023 International Conference on Control, Communication and Computing (ICCC)*, 1–5. IEEE.

Li, Z., Zhou, L., and Wang, J. (2021). Active disturbance rejection current control for synchronous reluctance motor. In *2021 IEEE 4th Student Conference on Electric Machines and Systems (SCEMS)*, 1–5. IEEE.

Scalcon, F.P. et al. (2019). Contribuições ao acionamento e controle dos motores de relutância variável e síncrono de relutância.

Zhou, W. and Gao, Z. (2007). An active disturbance rejection approach to tension and velocity regulations in web processing lines. In *2007 IEEE International Conference on Control Applications*, 842–848. IEEE.